Guiding Electron Emissions by Excess Negative Charges in Multiply Charged Molecular Anions

Chuan-Gang Ning, Phuong Diem Dau, and Lai-Sheng Wang*

Department of Chemistry, Brown University, Providence, Rhode Island 02912, USA

(Received 8 October 2010; published 22 December 2010)

Using photoelectron imaging, we show the effects of excess negative charges on the directions of outgoing electrons in multiply charged anions. Photoemissions are observed to occur either in a perpendicular or parallel direction, depending on the molecular configurations and origins of the detached electrons. Detachment of the π electrons from biphenyl-disulfonate dianions is shown to occur in a perpendicular direction due to the Coulomb repulsion from the two terminal charges, whereas detachment from the sulfonate groups in linear aliphatic disulfonates occurs in parallel directions.

DOI: 10.1103/PhysRevLett.105.263001 PACS numbers: 33.80.Eh, 36.90.+f

Although multiply charged anions (MCAs) are ubiquitous in the condensed phase, isolated MCAs are usually not stable due to the strong intramolecular Coulomb repulsion and are difficult to form in the gas phase [1–7]. Electrospray [8] was shown to be an efficient method to transport MCAs from solution samples to the gas phase [9,10]. The coupling of electrospray with photoelectron spectroscopy has allowed MCAs to be spectroscopically characterized for the first time [11–13]. When an electron is detached from an MCA, it experiences a short-range attraction by the nuclei and a long-range repulsion from the negatively charged residual ion, giving rise to the so-called repulsive Coulomb barrier (RCB). The RCB prevents slow photoelectrons from being emitted from MCAs, resulting in a cutoff in the photoelectron spectra of all MCAs [11–13]. The RCB provides dynamic stability to MCAs, allowing long-lived metastable MCAs with negative electron binding energies to be observed [14–16].

The strong intramolecular Coulomb repulsion and the RCB not only influence the energetics and stability of MCAs, but are also expected to influence the electron emission dynamics. Recently, we reported the first photoelectron imaging on MCAs to investigate the effects of the RCB on the outgoing electron angular distribution [17,18]. Photoelectron imaging yields electron angular distributions and kinetic energies at the same time [19–22]. Using this technique, we observed for a series of linear dicarboxylate dianions there is a maximum detachment cross section when the dianions are aligned with the laser polarization [17,18]. Because electron detachment occurs from the terminal $-CO_2^-$ groups, parallel electron distributions are observed due to the Coulomb repulsion from the remaining charge to the outgoing electrons [Fig. 1(a)]. However, if a system can be found, in which electron detachment occurs from the central part of a linear doubly charged anion, one would expect a perpendicular electron emission pattern owing to the Coulomb repulsion from the two terminal charges [Fig. 1(b)]. Here we report the observation of a perpendicular electron emission pattern from the diphenyl disulfonate dianion, in which the highest occupied molecular orbital (HOMO) consists of the π system on the phenyl rings. Electrostatic potentials and the RCBs are calculated, confirming the experimental observations and showing how the directions of the outgoing electrons are dictated by the excess charges.

The experiments were performed on an electrospray photoelectron apparatus equipped with a velocity-map imaging detector [18,23]. Sulfonate-containing MCAs were produced by electrospray, selected by a time-of-flight mass analyzer, and photodetached by a laser beam in the interaction zone of a velocity-map imaging system [18,19]. The ejected photoelectrons were projected onto a phosphor screen behind a set of microchannel plates and recorded by a CCD camera. The raw imaging data were reconstructed through an inverse Abel transformation [24,25]. The experiment was calibrated by the known spectra of Br^- and I^-. The typical energy resolution was about 40 meV for 1.5 eV electrons [18].

Figure 2 shows the results for biphenyl disulfonate ($BPDS^{2-}$) at two photon energies. The reconstructed photoelectron images [Figs. 2(b) and 2(e)] display maxima at directions perpendicular to the laser polarization. The

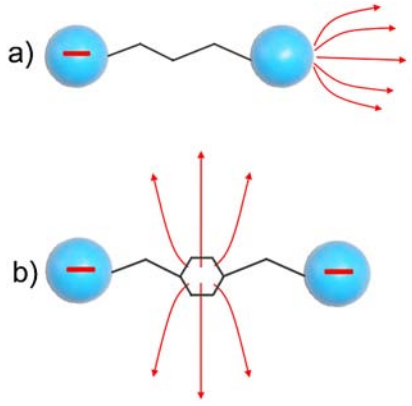

FIG. 1 (color online). Schematics showing a parallel electron distribution (a) and a perpendicular distribution (b) as a result of electron detachment from different parts of a doubly charged anion.

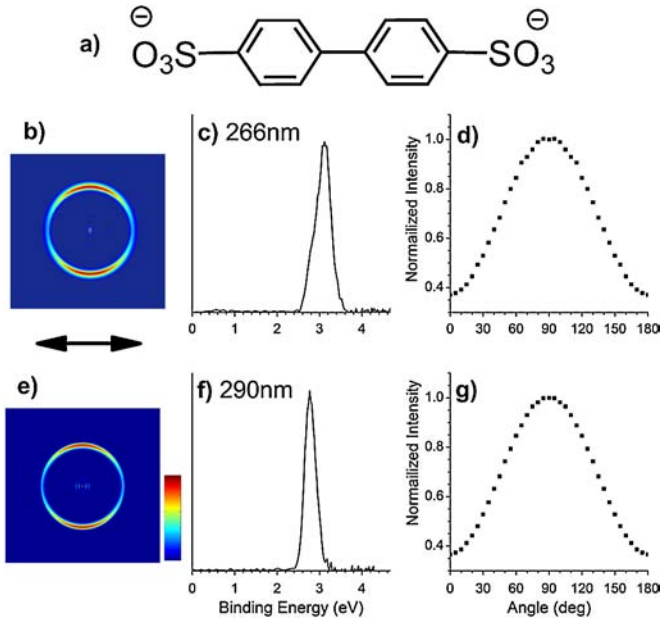

FIG. 2 (color online). Photoelectron imaging of biphenyl disulfonate ($BPDS^{2-}$). (a) Molecular structure of $BPDS^{2-}$. (b) Photoelectron image at 266 nm (4.661 eV) after inverse Abel transformation. The double arrow represents the laser polarization directions and the color bar represents the intensity scale. (c) Electron binding energy spectrum at 266 nm. (d) Photoelectron angular distribution at 266 nm. (e) Photoelectron image at 290 nm (4.275 eV) after inverse Abel transformation. (f) Electron binding energy spectrum at 290 nm. (g) Photoelectron angular distribution at 290 nm.

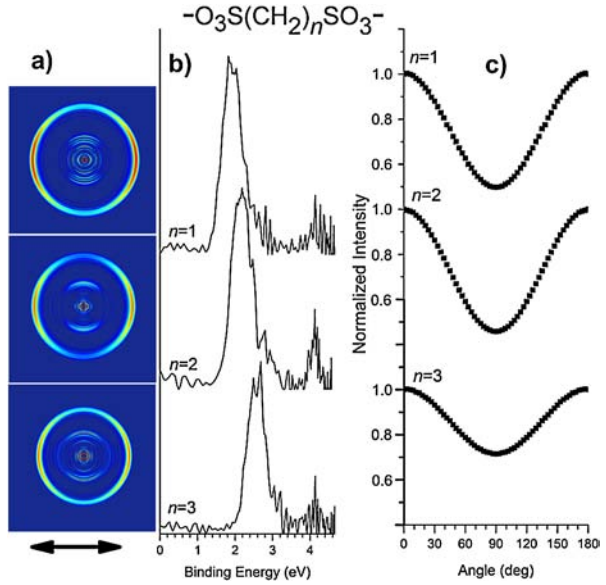

FIG. 3 (color online). Photoelectron imaging of $^{-}O_3S(CH_2)_nSO_3^{-}$ (DS_n^{2-}, $n = 1$–3) at 266 nm. (a) Photoelectron images. The low kinetic energy signals are likely due to detachment of the monoanion product by a second photon. (b) Electron binding energy spectra. (c) Photoelectron angular distributions.

binding energy spectra were obtained by integrating photoelectron signals at all angles. At 266 nm (4.661 eV), we only observed one detachment band due to the high electron binding energies and the high RCB. The measured adiabatic electron binding energy for $BPDS^{2-}$ is 2.6 eV and the estimated RCB from the spectral cutoff at 3.4 eV is 1.3 eV ($h\nu - 3.4$ eV). This result was consistent with the fact that we could not observe electron emission using 355 nm (3.496 eV) photons due to the RCB. We were able to observe photoemission at 290 nm (4.275 eV) using a dye laser [Fig. 2(e)] and the observed cutoff at 3.0 eV gave rise to the same RCB (1.3 eV) as obtained from the 266 nm (4.661 eV) spectrum. Figures 2(d) and 2(g) shows the angular distributions relative to the laser polarization, normalized to one as the maximum intensity (only data from 0°–180° are displayed because of symmetry). The angular distributions at both photon energies are similar, exhibiting maximum intensities at directions perpendicular to the laser polarization and minimum intensities in the parallel directions.

This was an interesting observation. If the electron detachment occurred from the terminal $-SO_3^-$ groups, we expected to see a parallel angular distribution due to the Coulomb repulsion from the remaining charge on the opposite end of the molecule, as previously observed for the linear dicarboxylate dianions, $^{-}O_2C(CH_2)_nCO_2^{-}$ ($n = 3$–11) [17,18]. Because the electron binding energy of the $-SO_3^-$ group is much higher than that of $-CO_2^-$, our observation suggests that the HOMO of $BPDS^{2-}$ may be the π system of the diphenyl group. If electron detachment is from the middle part of the molecule, we would expect the two terminal negative charges to force the electron to be emitted perpendicular to the molecular axis [Fig. 1(b)]. To test this conjecture, we performed control experiments on a series of linear disulfonate dianions, $^{-}O_3S(CH_2)_nSO_3^{-}[DS_n^{2-}]$ ($n = 1$–3) [Fig. 3)]. We only observed one band for all three species at 266 nm due to the high electron binding energies and the high RCB. In fact, the 266 nm photons were below the RCB and the observed signals were all due to electron tunneling [26], consistent with the extremely low detachment cross sections. It can be seen that the electron binding energies increase as the chain length increases, while the cutoff induced by the RCB decreases. Most importantly, the photoelectron intensities are peaked along the laser polarization for all three DS_n^{2-} dianions [Figs. 3(a) and 3(c)], as expected.

Further support for the above interpretation was provided by photoelectron imaging of the bisdisulizole tetraanion ($BDSZ^{4-}$) [Fig. 4]. The strong intramolecular Coulomb repulsion induces a negative electron binding energy of -0.6 eV for $BDSZ^{4-}$, reminiscent of the phthalocyanine tetrasulfonate with a binding energy of -0.9 eV [14]. The spectral cutoff yields a RCB of $\sim$3.3 eV for $BDSZ^{4-}$. The two detachment bands observed for

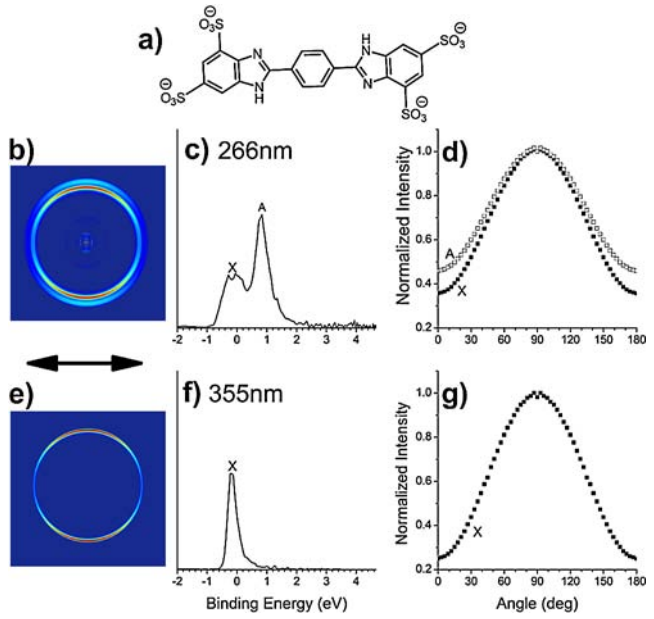

FIG. 4 (color online). Photoelectron imaging of bisdisulizole tetraanion ($BDSZ^{4-}$). (a) Molecular structure of $BDSZ^{4-}$. (b) Photoelectron image at 266 nm after inverse Abel transformations. (c) Electron binding energy spectrum. (d) Photoelectron angular distributions for the X and A bands at 266 nm. (e) Photoelectron image after inverse Abel transformation at 355 nm (3.496 eV). (f) Electron binding energy spectrum at 355 nm. (g) Photoelectron angular distribution at 355 nm.

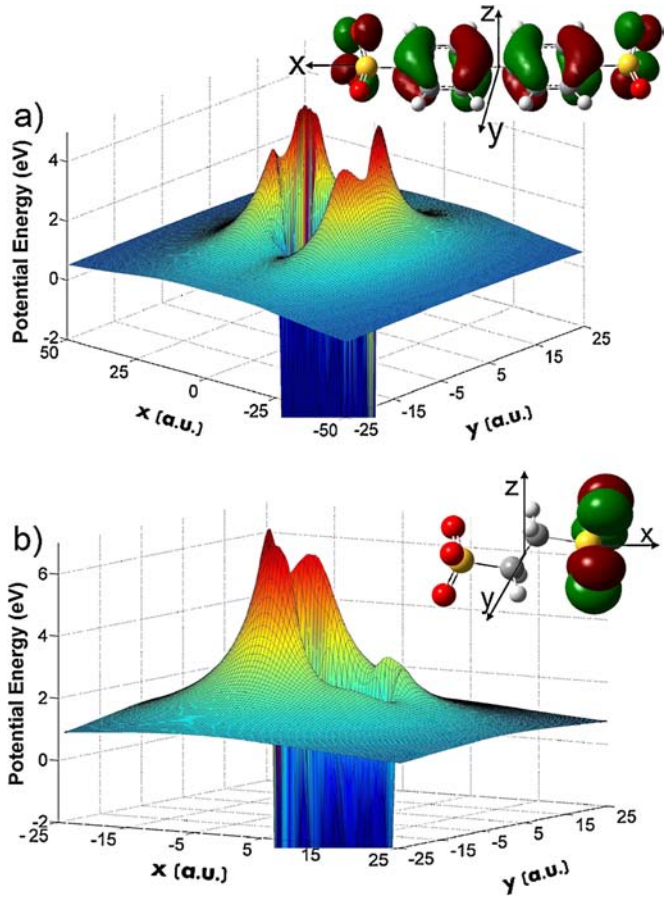

FIG. 5 (color online). Calculated electrostatic potential surface experienced by removing a HOMO electron from $BPDS^{2-}$ (a) and from $DS_2{}^{2-}$ (b). The inset shows the HOMO and the coordinate system for each anion.

$BDSZ^{4-}$ both display strong perpendicular distributions, suggesting that they are due to the π systems of the aromatic rings or the N lone pairs. Our prior studies on several aromatic tri- or tetrasulfonate anions [16,27] showed that the HOMOs of these anions are the π orbitals due to both the high electron binding energies of the sulfonate and the relatively low electron binding energies of the π electrons.

To understand quantitatively how the intramolecular Coulomb repulsions influence the photodetachment processes in MCAs, we calculated the RCBs for $BPDS^{2-}$ and $DS_2{}^{2-}$. The RCB is a highly anisotropic quantity and is dependent on the molecular structures. In the frozen orbital static approximation developed by Dreuw and Cederbaum [28], the electrostatic potential experienced by an outgoing electron detached from the νth orbital is expressed as

$$V_\nu(r) = -\sum_{i=1}^{K} \frac{Z_i}{|R_i - r|} + \sum_{j=1, j\neq\nu}^{N} \int \frac{\phi_j^* \phi_j}{|r_j - r|} d\tau \quad (1)$$

where the first term is the attraction between the outgoing electron and the K nuclei and the second term corresponds to the repulsion between the outgoing electron and the remaining $N-1$ electrons. The electron density distribution $\phi_j^* \phi_j$ for each molecular orbital ϕ_j was calculated using density functional theory at the level of B3LYP–Aug-cc-pVTZ in GAUSSIAN03.

Figure 5(a) shows the calculated potential energy surface for detaching an electron from the HOMO of $BPDS^{2-}$. The inset displays the coordinate system and the HOMO picture, which is indeed a π orbital mainly localized on the aromatic rings of $BPDS^{2-}$. The electrostatic potential is three dimensional: Fig. 5(a) displays a cross section on the molecular plane defined by the two benzene rings. The strong Coulomb repulsions from the terminal charges are clearly seen, forming the two high potential barriers (the highest barrier is 5.1 eV). The lowest potential barrier is along the y axis, which is perpendicular to the axis connecting the two $-SO_3{}^-$ groups. The lowest barrier along the y axis is 1.2 eV, in excellent agreement with the observed RCB of ~1.3 eV. Clearly, if the kinetic energy of the outgoing electron is lower than the electrostatic repulsions by the terminal negative charges, the electron will be forced to escape from the lowest valley formed by the Coulomb corral of the two terminal charges, yielding the observed perpendicular angular distributions.

For the $DS_n{}^{2-}$ dianions, our calculations showed that the HOMO consisted of two degenerate molecular orbitals,

mainly from the O_{2p} orbitals of the $-SO_3^-$ groups. A linear transformation of the two degenerate orbitals resulted in two localized orbitals, one on each SO_3^- group [see inset of Fig. 5(b)]. As a result, the electrostatic potential for removing an electron from the HOMO of DS_n^{2-} is quite different from that of $BPDS^{2-}$, as shown in Fig. 5(b) for $n = 2$. The remaining charge creates a high potential barrier (6.7 eV at the highest potential) for the outgoing electron and pushes it along the molecular axis, yielding the parallel angular distributions.

In conclusion, photoemission has been observed to be guided by the excess charges in multiply charged anions. Using photoelectron imaging, we have obtained angular distributions of a series of sulfonate-containing multiply charged anions. Electron emission from terminal sites was observed to exhibit parallel distributions, whereas electron detachment from the central part of multiply charged anions display perpendicular distributions owing to the strong Coulomb repulsion from the surrounding negative charges. Therefore, photoelectron imaging may be used to obtain information about charge distributions and the molecular structures of complex anions.

This work was supported by NSF (CHE-1036387).

*Lai-Sheng_Wang@brown.edu

[1] S. N. Schauer, P. Williams, and R. N. Compton, Phys. Rev. Lett. **65**, 625 (1990).
[2] J. Kalcher and A. F. Sax, Chem. Rev. **94**, 2291 (1994).
[3] M. K. Scheller, R. N. Compton, and L. S. Cederbaum, Science **270**, 1160 (1995).
[4] A. I. Boldyrev, M. Gutowski, and J. Simons, Acc. Chem. Res. **29**, 497 (1996).
[5] G. R. Freeman and N. H. March, J. Phys. Chem. **100**, 4331 (1996).
[6] L. S. Wang and X. B. Wang, J. Phys. Chem. A **104**, 1978 (2000).
[7] A. Dreuw and L. S. Cederbaum, Chem. Rev. **102**, 181 (2002).
[8] J. B. Fenn, Angew. Chem., Int. Ed. Engl. **42**, 3871 (2003).
[9] A. T. Blades and P. Kebarle, J. Am. Chem. Soc. **116**, 10761 (1994).
[10] T. C. Lau *et al.*, J. Chem. Soc. Chem. Commun. 1487 (1994).
[11] L. S. Wang *et al.*, Phys. Rev. Lett. **81**, 2667 (1998).
[12] X. B. Wang, C. F. Ding, and L. S. Wang, Phys. Rev. Lett. **81**, 3351 (1998).
[13] O. T. Ehrler *et al.*, Phys. Rev. Lett. **91**, 113006 (2003).
[14] X. B. Wang and L. S. Wang, Nature (London) **400**, 245 (1999).
[15] K. Arnold *et al.*, J. Phys. Chem. A **107**, 794 (2003).
[16] X. B. Wang *et al.*, J. Am. Chem. Soc. **131**, 9836 (2009).
[17] X. P. Xing, X. B. Wang, and L. S. Wang, Phys. Rev. Lett. **101**, 083003 (2008).
[18] X. P. Xing, X. B. Wang, and L. S. Wang, J. Chem. Phys. **130**, 074301 (2009).
[19] A. Eppink and D. H. Parker, Rev. Sci. Instrum. **68**, 3477 (1997).
[20] E. Surber and A. Sanov, J. Chem. Phys. **116**, 5921 (2002).
[21] A. Osterwalder *et al.*, J. Chem. Phys. **121**, 6317 (2004).
[22] S. J. Cavanagh *et al.*, Phys. Rev. A **76**, 052708 (2007).
[23] L. S. Wang *et al.*, Rev. Sci. Instrum. **70**, 1957 (1999).
[24] V. Dribinski *et al.*, Rev. Sci. Instrum. **73**, 2634 (2002).
[25] G. A. Garcia, L. Nahon, and I. Powis, Rev. Sci. Instrum. **75**, 4989 (2004).
[26] X. B. Wang, C. F. Ding, and L. S. Wang, Chem. Phys. Lett. **307**, 391 (1999).
[27] J. Yang *et al.*, J. Chem. Phys. **128**, 091102 (2008).
[28] A. Dreuw and L. S. Cederbaum, Phys. Rev. A **63**, 049904 (E) (2001).